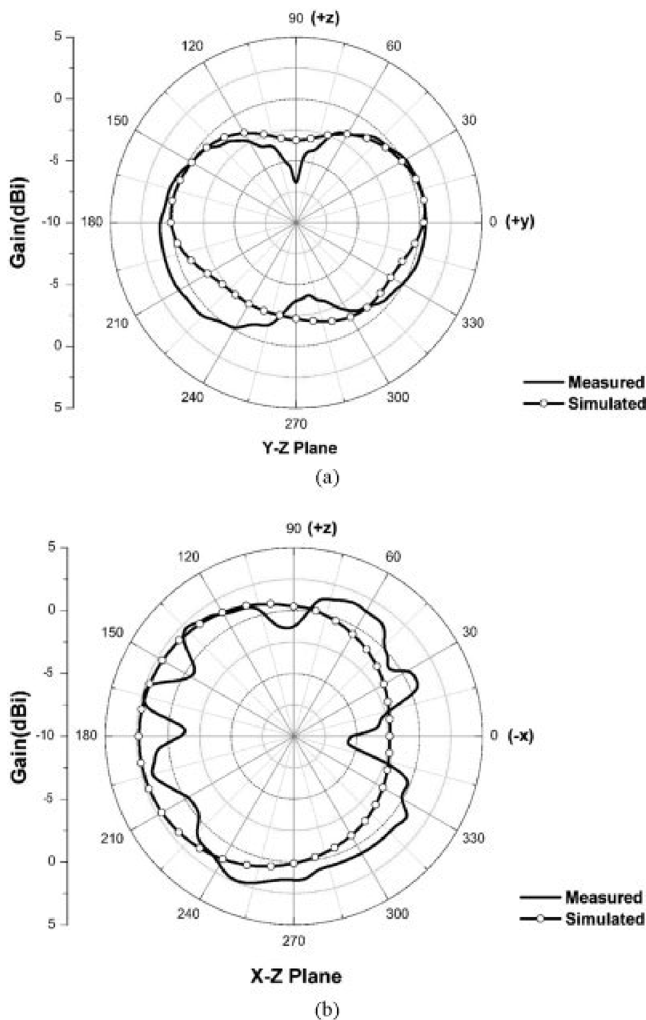

Figure 5 (a) Radiation pattern of the antenna at 5.8 GHz when $\varphi = 0°$; (b) radiation pattern of the antenna at 5.8 GHz when $\varphi = 90°$

gain is about 0.5 dB and gain variation is less than 0.3 dB. It can fulfill the requirements for most of the indoor wireless applications and the relative low gain at the 2.4-GHz band is mainly caused by the cancellation of the meandering to achieve small size.

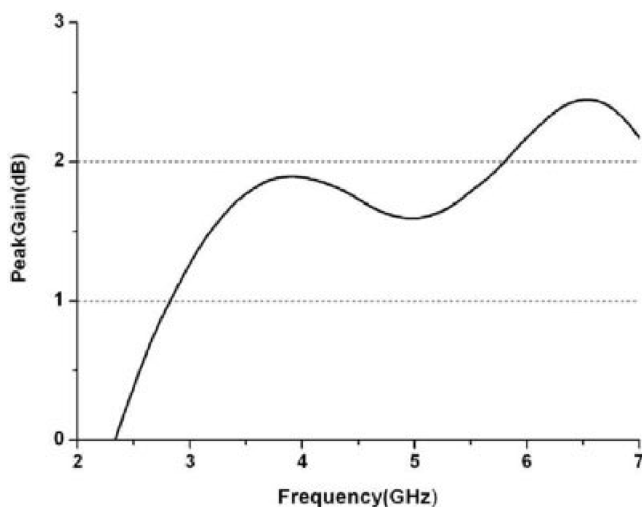

Figure 6 Peak gain of the proposed antenna

4. CONCLUSIONS

A compact dual-band 2.4/5-GHz T-slot antenna has been proposed and studied experimentally. This proposed antenna has a compact size (20 mm by 50 mm) and is composed of two orthogonal slots. With the use of the two orthogonal slots, the impedance bandwidth of the proposed antenna effectively covers both WLAN bands (2.4–2.5 GHz, 5.15–5.825 GHz), and the gain of the antenna can fulfill the requirements of most indoor wireless applications.

ACKNOWLEDGMENTS

We are grateful to Prof. Lixin Ran and Dr. Yu Yuan at Electromagnetics Academy, Zhejiang University, for their kind help.

REFERENCES

1. C.M. Su, H.T. Chen, F.S. Chang, and K.L. Wong, Dual-band slot antenna for 2.4/5.2 GHz WLAN operation, Microwave Opt Technol Lett 35 (2002), 306–308.
2. J.W. Wu, 2.4/5-GHz dual-band triangular slot antenna with compact operation, Microwave Opt Technol Lett 45 (2005), 81–84.
3. W.C. Liu, Broadband dual-frequency cross-shaped slot CPW-fed monopole antenna for WLAN operation, Microwave Opt Technol Lett 46 (2005), 353–355.
4. H.M. Hsiao, J.W. Wu, and Y.D. Wang, Novel dual-broadband rectangular-slot antenna for 24/5-GHz wireless communication, Microwave Opt Technol Lett 46 (2005), 197–201.
5. S.I. Latif, L. Shafai, and S.K. Sharma, Bandwidth enhancement and size reduction of microstrip slot antennas, IEEE Trans Antennas Propag 53 (2005), 994–1003.

© 2007 Wiley Periodicals, Inc.

NONLINEAR ACTUATION MODEL FOR LATERAL ELECTROSTATICALLY-ACTUATED DC-CONTACT RF MEMS SERIES SWITCHES

A. Lázaro,[1] D. Girbau,[2] L. Pradell,[2] and A. Nebot[2]
[1]Department of Electronics, Electrics and Automatic Engineering, Universitat Rovira i Virgili (URV), 43007, Av. Països Catalans, 26, Campus Sescelades, Tarragona, Spain
[2]Department of Signal Theory and Communications, Universitat Politècnica de Catalunya (UPC), Campus Nord UPC – Mòdul D3, Jordi Girona 1–3, 08034 Barcelona, Catalunya, Spain

Received 17 October 2006

ABSTRACT: *In this work, a nonlinear model to predict actuation characteristics in lateral electrostatically-actuated DC-contact MEMS switches is proposed. In this case a parallel-plate approximation cannot be applied. The model is based on the equilibrium equation for an elastic beam. It is demonstrated that the contribution of fringing fields is essential. The model relies on finite-difference discretization of the structures, applying boundary conditions and is solved with a Gauss-Seidel relaxation iteration scheme. Its usefulness is demonstrated in a series MEMS switch with lateral interdigital electrostatic actuation.* © 2007 Wiley Periodicals, Inc. Microwave Opt Technol Lett 49: 1238–1241, 2007; Published online in Wiley InterScience (www.interscience.wiley.com). DOI 10.1002/mop.22450

Key words: *MEMS; interdigital; electrostatic actuation; in-plane switch*

1. INTRODUCTION

The miniaturization of wireless communication systems is actually limited by off-chip passive elements. Among them, RF switches

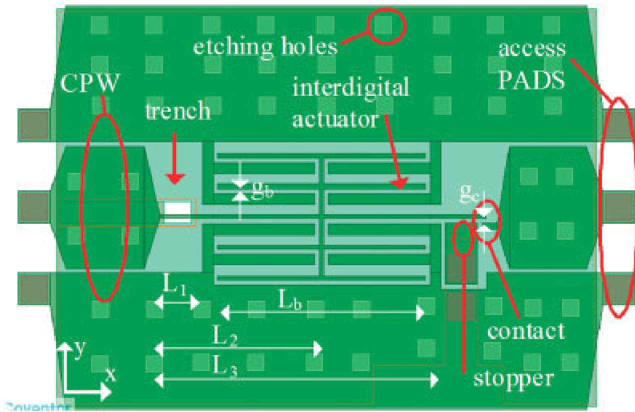

Figure 1 Switch top view. Its main building parts are pointed out. [Color figure can be viewed in the online issue, which is available at www.interscience.wiley.com]

are candidates to be replaced with their MEMS counterparts. Capacitive series and shunt MEMS switches (based on a metal–dielectric–metal contact) have been implemented in a number of applications, mainly at frequencies above 10–15 GHz [1]. Resistive-contact (or DC-contact) switches, based on a metal–metal contact, operate from DC to 30–40 GHz, covering perfectly the ground wireless communication bands, all of them under 6 GHz. Most resistive-contact switches, mainly when electrostatically actuated, have been implemented using out-of-plane movement, which is perpendicular to the substrate [2].

The need for high aspect ratio structures (thick elements with small gaps), capable of producing forces great enough to ensure a good switch contact with moderate actuation voltage has been the main drawback when implementing in-plane switches (lateral movement, parallel to substrate). In consequence, most of the few lateral RF switches proposed in the literature so far are electrothermally-actuated [3], a topology with inherent power consumption and packaging limitations. With the recent spectacular evolution of metal micromachining technology, manufacturing high aspect ratio structures is possible, which leave the way open for lateral electrostatically-actuated RF switches, as demonstrated in [4, 5].

However, an important problem arises with those devices, namely, a lack of available models for actuation fast prediction, since a parallel-plate approximation does not apply in this case, on the contrary to out-of-plane switches, where parallel-plate approximation has been used in most works as a first order model. Finite Element Analysis of these structures is adequate but time-consuming and, moreover, it requires accurate input data for a precise actuation simulation In consequence, it is essential to develop simpler models for a first, yet accurate, actuator design.

This letter presents a new model to reliably predict actuation characteristics in lateral electrostatically-actuated DC-contact MEMS series switches for operation in the ground wireless bands. The model is validated by using a series switch [5] manufactured with the multi project wafer process MetalMumps™ [6]. It is fabricated on a low-resistivity substrate (1–2 Ω cm), and a 25 μm deep trench is carved under the device to reduce substrate loss, resulting in a suspended switch.

2. SERIES SWITCH TOPOLOGY

Fig. 1. shows a top view of the designed switch that has been used to validate the model, where its main dimensions and building parameters are pointed out. The switch is made of nickel, based on a CPW series configuration and a resistive gold-gold contact. When no actuation voltage is applied, the switch is in its OFF state, while when a DC voltage is applied superposed to the RF signal, the interdigital actuator forces the moving tip to approach the fixed part. The initial gaps for contact and interdigital actuator are g_c = 5.2 μm and g_b = 5.7 μm, respectively. The minimum dimensions are fixed by the technology design rules, that being the main limit, along with the thickness of the suspended structure (only 20 μm), to decrease the actuation voltage. For this reason, an interdigital actuator topology along with a leverage bending technique are used in order to obtain a suitable switch actuation voltage. As a consequence, most of the structure is deflected less than the pull-in limit, when on contact.

3. ACTUATION MODEL

The parallel-plate approximation for this kind of switches (either interdigital or not) only applies for the initial position, being no longer useful when the mobile structure is actuated.

Then a nonlinear model for the structure has been developed, for fast and accurate prediction of the displacement, which is based on the equilibrium equation for an elastic beam [7]:

$$\frac{\partial^2}{\partial x^2}\left(E \cdot I \frac{\partial^2 y}{\partial x^2}\right) = F_{\text{elec}} \tag{1}$$

where (see Fig. 1) $y(x)$ is the beam lateral displacement, x is the distance along the beam length, E is the elastic modulus of nickel (beam material), $I = t{\cdot}w3/12$ is the moment of inertia of a straight beam with a rectangular cross section, w is the beam width, t is the beam height (thickness), and F_{elec} is the electrostatic force per unit length. This force is the sum of distributed electrostatic forces along the beam electrode ($L_1 < x < L_3$) and the force of N lateral beams (F_b) with length L_b and electrode gap g_b applied at point $x = L_2$.

$$F_{\text{elec}}(x) = -f_n(b(x))\frac{\varepsilon_0 t V^2}{2(g - y(x))^2}[u(x - L_1) - u(x - L_3)] + N \cdot F_b \delta(x - L_2) \tag{2}$$

$$F_b = \frac{-\varepsilon_0 t V^2}{2}\int_{x_{b1}}^{x_{b2}} \frac{f_n(b_b(x'))dx'}{(g_b - y(x'))^2} \tag{3}$$

where g is the electrode gap of the central beam, $b(x) = (g-y(x))/t$ is the gap/central beam height aspect ratio, $bb(x) = (g_b-y(x))/t$ is the gap/lateral beam height aspect ratio, $u(x)$ is the stepwise function, $\delta(x)$ is the delta function, ε_0 is the permittivity of free space, and V is the applied voltage. The model can be used in switches with only one lateral beam (N = 1) when thick structures are available or in an interdigital topology when the material thickness is limited (as in this work; N = 4). The capacitance is corrected for fringing fields ($C\ll = C{\cdot}f_n$, being C the parallel plate capacitance and $C\ll$ the fringing-field corrected capacitance) using the function $f_n(b)$ defined in [8], and:

$$f_n(b) = \begin{cases} 1 + 4.246b, & 0 \le b \le 0.005 \\ 1 + \sqrt{11.087b^2 + 0.001097}, & 0.005 < b \le 0.05 \\ 1 + 1.986b^{0.8258}, & b > 0.05 \end{cases} \tag{4}$$

Integral [3] can be solved numerically. If fringing fields are neglected ($f_n = 1$), we find

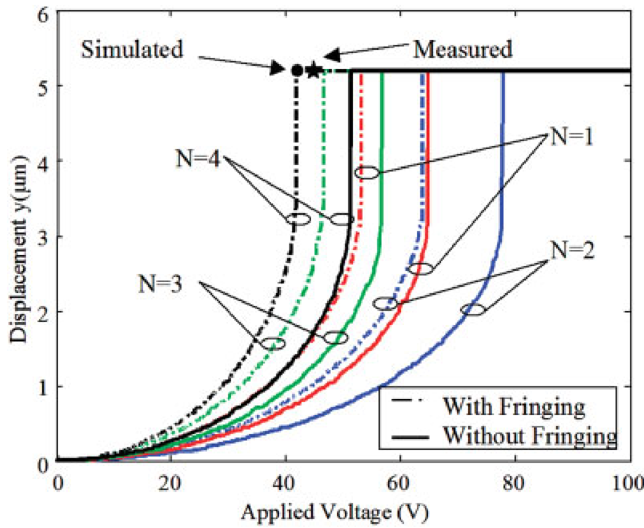

Figure 2 Displacement vs. voltage for $N = 1, 2, 3, 4$ interdigital beams. Simulated (●) and measured (←) points correspond to the manufactured actuator (Figs. 1 and 5). [Color figure can be viewed in the online issue, which is available at www.interscience.wiley.com]

$$F_b = \frac{\varepsilon_0 t V^2}{2\left(g_b - z(L_2) - \frac{L_b}{2}\tan\alpha\right)} - \frac{\varepsilon_0 t V^2}{2\left(g_b - z(L_2) + \frac{L_b}{2}\tan\alpha\right)} \quad (5)$$

where $t(x)$ represents the shape (height) of the actuation electrode (here assumed constant), α is the bending angle at point $x = L_2$ (obtained from derivate of the displacement, $\tan(\alpha) = dy/dx$ at $x = L_2$). The differential Eq (1) must be solved with boundary conditions: $y(x = 0) = y'(x = 0) = y''(x = L) = 0$. Using finite differences discretisation schema, we can obtain the following nonlinear equation system:

$$[M][y_i] = [F_{\text{elec}}(y_i)] \quad (6)$$

$$[M] = \frac{EI}{\Delta x^4}\begin{bmatrix} 7 & -4 & 1 & 0 & \cdots & \\ -4 & 6 & -4 & 1 & \cdots & \\ 1 & -4 & 6 & -4 & 1 & \cdots \\ & \cdots & 1 & -4 & 5 & -2 \\ & & & 1 & -2 & 1 \end{bmatrix} \quad (7)$$

where i is the mesh index, and Δx is the spacing between mesh points. One approach to solve the nonlinear system is to use a simple nonlinear Gauss–Seidel relaxation iteration scheme [9]. Assuming zero displacement as initial value for vector [yi], an initial force vector is calculated. Inverting [M], a new estimation of vector displacement is calculated. Then, the force in iteration k is updated from the last iteration using the following relaxation formula:

$$[F_{\text{elec}}]^k = [F_{\text{elec}}]^{k-1} + \omega([F_{\text{elec}}(y_i^k)] - [F_{\text{elec}}]^{k-1}) \quad (8)$$

being ω the relaxation factor (typically between 0.85 and 0.9). The procedure is repeated up to the desired residual error in the displacement is obtained. A more robust approach than non linear relaxation is to use a full-Newton method [9]:

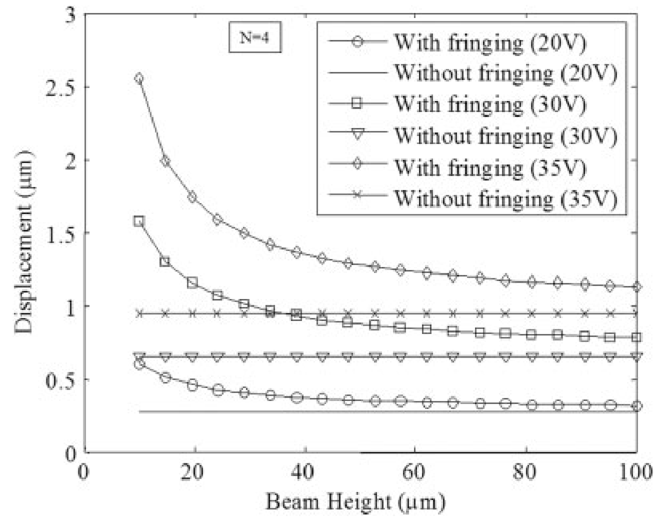

Figure 3 Displacement vs. beam height ($N = 4$)

$$[y_i]^k = [y_i]^{k-1} - \left([M] - \left[\frac{dF_{\text{elec}}}{dx}\right]^{k-1}\right)^{-1}([M][y_i]^{k-1} - [F_{\text{elec}}]^{k-1}) \quad (9)$$

At low voltages, the beam deflection is small, the coupling between the electrical and mechanical systems is weak, and the relaxation algorithm works very well. For higher voltages, the Newton algorithms converge much faster than the relaxation algorithm. Fig. 2 shows the maximum lateral displacement as a function of the applied voltage for several number of lateral beams including fringing corrections and without the corrections. The contact voltage (when displacement is equal to the gap contact, g_c) decreases with the number of lateral beams. Also, this figure shows the important effect of fringing capacitance. In fact, the increase of electrostatic force due fringing fields decreases the pull-in voltage. The model predicts a contact voltage of 42 V for $N = 4$ lateral beams including fringing effects and 52 V using parallel-plate capacitance (for the switch of Fig. 1). This value is in agreement with the experimental contact voltage, 45 V, that is within a 5% error. This difference may in part be justified by the overestimation of the electrostatic force caused by screening because of the

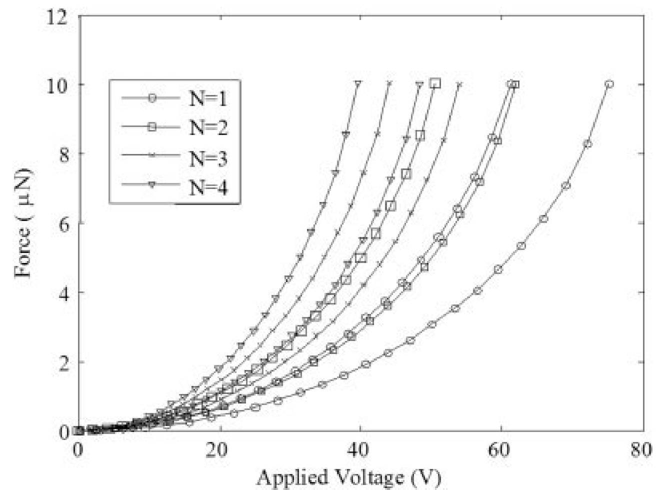

Figure 4 Force at the end of the beam vs. applied voltage

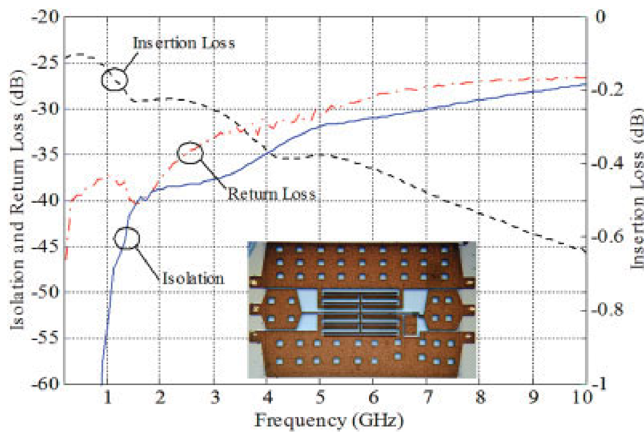

Figure 5 Measured insertion loss, return loss and isolation. [Color figure can be viewed in the online issue, which is available at www.interscience.wiley.com]

substrate and ground plane, reducing the contact voltage about 2 V in the simulations.

Fig. 3 shows the displacement as a function of the beam height. This displacement is independent of the beam height when fringing effects are neglected. However, when beam height decreases, the fringing capacitance increases resulting in an increase of the force and displacement for a given applied voltage. This result demonstrates again that to take into consideration fringing fields is essential in these structures. Finally, Fig. 4 shows the simulated force at the contact with and without the inclusion of fringing effects. This figure shows that fringing effects increase the capacitance and the force. This fact improves the contact reducing its resistance and the switch losses.

The measured performance of the manufactured device is shown in Fig. 5, along with its photograph [5]. Insertion loss is −0.13/−0.41 dB at 0.9/6 GHz, return loss is −37.7/−28.7 dB at 0.9/6 GHz and isolation is −60.2/−31 dB at 0.9/6 GHz. These results are comparable to the ones obtained in [4] on a high-resistivity silicon substrate.

4. CONCLUSIONS

A model for prediction of the actuator displacement in electrostatically actuated, lateral contact RF MEMS series switches has been presented, a switch topology with increasing acceptance due to the evolution of thick metal layers technology. It has been demonstrated that in this topology the parallel-plate approximation for actuator displacement can not be assumed. In addition, it has also been demonstrated the importance of considering fringing fields in the model for a reliable prediction. The simulated results match very well with the measured actuation characteristics of a series switch with electrostatic interdigital actuation manufactured with MetalMumps™.

ACKNOWLEDGMENT

This work was supported by the Spanish Government under Grants TIC2000–0144-P4–02 and ESP2004–07067-C03–03 (MCYT).

REFERENCES

1. J.B. Muldavin, G.M. Rebeiz, High-Isolation CPW MEMS shunt switches—Part 1: Modeling, IEEE Trans Microwave Theory Tech 48 (2000), 1045–1052.
2. D. Mercier, P.L. Charvet, P. Berruyer, C. Zanchi, L. Lapierre, O. Vendier, J.L. Cazaux, P. Blondy, A DC to 100 GHz high performance ohmic shunt switch, IEEE MTT-S Int Microwave Symp 3 (2004), 1931–1934.
3. Y. Wang, et al., A low-voltage lateral MEMS switch with high RF performance, IEEE J Microelectromech Syst 13 (2004), 902–911.
4. A.Q. Liu, M. Tang, A. Agarwal, A. Alphones, Low-loss lateral micromachined switches for high-frequency applications, J Micromech Microeng 15 (2005), 157–167.
5. D. Girbau, L. Pradell, A. Lázaro, A. Nebot, In-plane Electrostatically-Actuated RF MEMS Switch Suspended on a Low-Resistivity Substrate," 36th European Microwave Conference; Manchester (UK), Sept. 2006, 505–508.
6. Cowen, B. Dudley, E. Hill, et al., MetalMUMPs Design Handbook, Rev. 1.0. http://www.memsrus.com/nc-mumps.metal.html.
7. Klaus-Jürgen Bathe, Finite Element Procedures in Engineering Analysis, Prentice-Hall, 1982.
8. H. Nishiyama, M. Nakamura, Capacitance of a Strip Capacitor, IEEE Trans Components, Hybrids, Manuf Tech 13 (1990), 417–423.
9. W.H. Press, B.P. Flannery, S.A. Teukolsky, et al., Numerical Recipes in C, 2nd ed., Cambridge University Press, 1992.

© 2007 Wiley Periodicals, Inc.

A CMOS POWER AMPLIFIER WITH AN ADAPTIVE BIAS SCHEME FOR MOBILE RADIO FREQUENCY IDENTIFICATION READER APPLICATIONS

Jeonghu Han, Younsuk Kim, Changkun Park, Dongho Lee, and Songcheol Hong
Department of Electrical Engineering and Computer Science, Korea Advanced Institute of Science and Technology, 373–1 Guseong-Dong, Yuseong-Gu, Daejeon 305–701, Korea

Received 23 October 2006

ABSTRACT: *A 900-MHz linear power amplifier with an adaptive bias scheme is fabricated using a 0.25-μm CMOS technology. The power amplifier operates over the range of 860–960 MHz, which is the ultra-high-frequency band for radio frequency identification (RFID). All matching networks and RF chokes are implemented on a chip. The developed power amplifier provides a 1-dB-gain-compression point* ($P_{1\ dB}$) *of 27 dBm and a power-added-efficiency (PAE) of 28% at the* $P_{1\ dB}$. *The adaptive bias scheme enables the power amplifier to reduce the quiescent power consumption from 280 to 80 mW by adjusting the gate voltage of power transistors as a function of the input power.* © 2007 Wiley Periodicals, Inc. Microwave Opt Technol Lett 49: 1241–1245, 2007; Published online in Wiley InterScience (www.interscience.wiley.com). DOI 10.1002/mop.22435

Key words: *adaptive bias; CMOS power amplifiers; transmission-line transformer; linear power amplifiers; radio frequency identification (RFID)*

1. INTRODUCTION

Radio frequency identification (RFID) is a wireless technology that allows a reader to activate and communicate with IC-tags on remote objects using radio waves. In today's industry, advanced end-user applications require RFID readers to be embedded into personal mobile devices [1]. Current efforts are therefore directed to developing a fully integrated, single-chip CMOS solution for a mobile RFID system. Implementing a power amplifier is one of the most difficult issues for single-chip design. Because of the low breakdown voltage and the substrate loss in CMOS processes, it is challenging to design a fully integrated CMOS power amplifier with high output power,